Remote Sensing of Environment 115 (2011) 876–886

Contents lists available at ScienceDirect

Remote Sensing of Environment

journal homepage: www.elsevier.com/locate/rse

Comparison of fire temperature and fractional area modeled from SWIR, MIR, and TIR multispectral and SWIR hyperspectral airborne data

Philip E. Dennison *, D. Scott Matheson

Department of Geography, University of Utah, 260 S Central Campus Dr., Room 270, Salt Lake City, UT 84112 USA

ARTICLE INFO

Article history:
Received 6 September 2010
Received in revised form 3 November 2010
Accepted 23 November 2010
Available online 17 December 2010

Keywords:
Fire
Temperature modeling
Spectral mixture modeling
Radiative transfer
AVIRIS
MASTER

ABSTRACT

Spectral mixture modeling has previously been used to retrieve fire temperature and fractional area from multiband radiance data containing emitted radiance from fires. While this type of temperature modeling has potential for improving understanding of fire behavior and emissions, modeled temperature and fractional area may depend on the wavelength region used for modeling. Using airborne hyperspectral (Airborne Visible Infrared Imaging Spectrometer; AVIRIS) and multispectral (MODIS/ASTER Airborne Simulator; MASTER) data acquired simultaneously over the 2008 Indians Fire in California, we examined changes in modeled fire temperature and fractional area that occurred when input wavelength regions were varied. Temperature and fractional area modeled from multiple MASTER runs were directly compared. Incompatible spatial resolutions prevented direct comparison of the AVIRIS and MASTER model runs, so total area modeled at each temperature was used to indirectly compare temperature and fractional area retrieved from these two sensors. AVIRIS and MASTER model runs using shortwave infrared (SWIR) bands produced consistent fire temperatures and fractional areas when modeled temperatures exceeded 800 K. Temperatures and fire fractional areas were poorly correlated for temperatures below 800 K and when the SWIR bands were excluded as model inputs. The single temperature blackbody assumption commonly used in mixing model retrieval of fire temperature is potentially useful for modeling higher temperature fires, but is likely not valid for lower temperature smoldering combustion due to mixed radiance from multiple fuel elements combusting at different temperatures. SWIR data contain limited emitted radiance from combustion at lower temperatures, and are thus essential for consistent modeling of fire temperature and fractional area at higher fire temperatures.

1. Introduction

Measuring fire properties using remotely sensed data is fundamentally a spectral mixing problem. The radiance measured by a sensor will be a combination of emitted radiance and reflected solar radiance contributed by the fire, background, and atmosphere. The relative contributions of emitted radiance and reflected solar radiance will vary depending on wavelength, the emissive properties of the fire and background, and the size of the fire relative to the area of measurement. Spectral mixture modeling can be used to separate contributions of radiance emitted by a fire from background emitted and reflected radiance, allowing retrieval of the fire's *effective* temperature and fractional area within a pixel (Dennison et al., 2006; Dozier, 1981). The general form of a spectral mixing model used for mixed spectral radiance (L_λ) is:

$$L_\lambda = \sum_{i=1}^{N} f_i L_{i\lambda} + \varepsilon_\lambda \tag{1}$$

where $L_{i\lambda}$ is the radiance of endmember i at wavelength λ, f_i is the fraction of endmember i, N is the number of endmembers, and ε_λ is the residual error. The modeled fractions of the endmembers are constrained by:

$$\sum_{i=1}^{N} f_i = 1 \tag{2}$$

These equations are the basis for a variety of fire temperature retrieval algorithms that have been used on airborne and spaceborne remotely sensed data (Dennison et al., 2006; Dozier, 1981; Eckmann et al., 2008, 2009, 2010; Matson & Holben, 1987; Oertel et al., 2004; Riggan et al., 2004; Wooster et al., 2003; Zhukov et al., 2005).

Fire temperature is an important control on carbon dioxide, carbon monoxide, and aerosol emissions from fires (Andreae & Merlet, 2001). Fire temperature indicates the dominance of flaming or smoldering combustion, which determines combustion efficiency and emissions of trace gasses (Palacios-Orueta et al., 2005). Fire temperature and duration can also impact soil chemistry, seed survival, and vegetation regrowth after fire (Brooks, 2002; DeBano, 2000; Drewa et al., 2002; Odion & Davis, 2000). Spatial remote measurement of fire temperature could greatly benefit understanding of fire processes, but the

* Corresponding author. Tel.: +1 801 585 1805.
E-mail address: dennison@geog.utah.edu (P.E. Dennison).

0034-4257/$ – see front matter © 2010 Elsevier Inc. All rights reserved.
doi:10.1016/j.rse.2010.11.015

complexity of collecting *in situ* data in fires and scaling from combusting fuel elements to spatial resolutions used for remote sensing makes it difficult to assess whether mixing model approaches can provide valid measurements of fire temperature. While the validity of fire temperature modeling cannot be confirmed using currently available data, the consistency of modeling can be assessed by comparing temperature and fire fractional area retrieved from different datasets acquired at the same time over the same fire. Using airborne hyperspectral and multispectral remotely sensed data covering the shortwave infrared (SWIR), mid-infrared (MIR) and thermal infrared (TIR) regions of the spectrum, this paper evaluates whether multiple endmember spectral mixture analysis (MESMA; Roberts et al., 1998) produces consistent temperatures and fractional areas across multiple spectral regions and two spatial resolutions. The results of this analysis provide a valuable demonstration of the abilities and limitations of spectral mixture modeling for retrieving fire properties, and offer insight into areas where further research on fire temperature modeling is needed.

2. Background

Total spectral radiance measured by a sensor over a daytime fire will be a combination of radiances from multiple sources. Wavelength-specific, at-sensor radiance ($L_{\lambda sensor}$) can be expressed as:

$$L_{\lambda sensor} = t_\lambda \left(L_{\lambda\rho} + L_{\lambda Ef} + L_{\lambda Eb} \right) + L_{\lambda P} \tag{3}$$

where t_λ is atmospheric transmittance, $L_{\lambda\rho}$ is reflected solar radiance at the surface, $L_{\lambda Ef}$ is fire emitted radiance at the surface, and $L_{\lambda Eb}$ is background emitted radiance at the surface. $L_{\lambda P}$ is path radiance, which is a function of atmospheric scattering of reflected and emitted radiances and atmospheric emission. The contribution of each of these terms is dependent on wavelength. Reflected solar radiance will strongly contribute to at-sensor radiance in the visible (0.4–0.7 μm), near infrared (NIR; 0.7–1.4 μm), and SWIR (1.4–2.5 μm) regions of the spectrum, but will be a minor contributor to at-sensor radiance in the TIR (8–14 μm) region of the spectrum. Radiance emitted by surfaces at background surface temperatures (~270–340 K) will not be significant in the visible, NIR, or SWIR, but can be an important source of radiance in the TIR. In the MIR (3–5 μm), all of these sources can have significant contributions to total radiance measured in a daytime image containing a fire.

Radiance emitted by fires and by surfaces at background temperatures is controlled by temperature (T), wavelength, and spectral emissivity (ε_λ). Emitted spectral radiance ($L_{\lambda E}$) can be calculated using Planck's equation:

$$L_{\lambda E} = \beta(\lambda, T) = \varepsilon_\lambda \frac{2hc^2}{\lambda^5 \left(e^{\frac{hc}{k\lambda T}} - 1 \right)} \tag{4}$$

where β represents the Planck equation as a function of wavelength and temperature, c is the speed of light, h is Planck's constant, and k is Boltzmann's constant. As temperature increases, emitted radiance increases and peak emission shifts to shorter wavelengths (Fig. 1). Blackbody emitters with relatively low kinetic temperatures dominantly emit in the TIR region of the spectrum, while strong emission in the SWIR occurs at temperatures commonly found in wildfires (Dennison et al., 2006).

Eq. (4) is the basis for the spectral mixing equation proposed by Dozier (1981) for modeling fire temperature and fire fractional area from MIR and TIR remotely sensed data. For the Dozier (1981) equation, at-sensor radiance is modeled as a sum of fire and background emitted blackbody radiances:

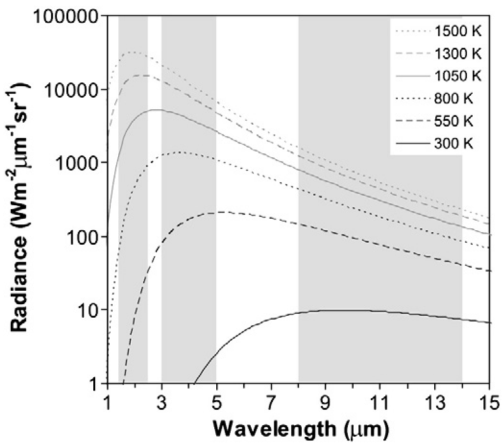

Fig. 1. Blackbody emission curves for a range of temperatures. The light gray bars represent (from left to right) the SWIR, MIR, and TIR spectral regions.

$$L_{\lambda sensor} = L_{\lambda Ef} + L_{\lambda Eb} = f_f \beta\left(\lambda, T_f\right) + f_b \beta(\lambda, T_b) \tag{5}$$

where f_f is the fire fractional area, f_b is the background fractional area, T_f is the fire temperature, and T_b is the background temperature. The fire fractional area and background fractional area are percentages of a whole pixel, and sum to 1. With two or more spectral bands, the set of equations for each band based on Eq. (5) can be solved simultaneously to estimate fire temperature and fire fractional area. Atmospheric absorption and path radiance are assumed to be minimal. Giglio and Kendall (2001) assessed the sensitivity of the Dozier (1981) temperature retrieval algorithm to atmospheric transmittance, instrument noise, path radiance, emissivity, and multiple emitting temperatures, and found significant variation in modeled temperature and fractional area at low fire fractional area values. Giglio and Justice (2003) examined how temperature and fractional area modeled by the Dozier (1981) algorithm vary with input wavelengths. Assuming emitted radiance contributions from both smoldering (600 K) and flaming (1000 K) combustion, they found large differences in retrieved temperature occurred when short wavelength (1.6–3.8 μm) and long wavelength (2.4–11.0 μm) bands were varied in a two band model. Modifications of the Dozier (1981) algorithm have been used to retrieve fire temperature from Advanced Very High Resolution Radiometer (AVHRR) data (Matson & Holben, 1987), airborne radiometer data (Riggan et al., 2004), and Bi-spectral InfraRed Detection (BIRD) data (Oertel et al., 2004; Wooster et al., 2003; Zhukov et al., 2005).

Dennison et al. (2006) introduced a multiple endmember spectral mixing approach to modeling fire temperature and fractional area. Multiple endmember spectral mixture analysis (MESMA; Roberts et al., 1998) allows the identity of endmembers to vary to find the set of endmembers that fits each modeled spectrum with the lowest root mean square error (RMSE). By using a combination of modeled emitted radiance and shade endmembers, and image reflected (and/or emitted) radiance endmembers, the multiple endmember approach described by Dennison et al. (2006) accounts for atmospheric scattering and does not assume that the background is a blackbody emitter. However, this approach still assumes that fire emission can be described using single temperature blackbody emitted radiance. One significant advantage of allowing multiple background endmembers is that this technique simultaneously produces a map of background land cover in addition to fire temperature and fractional area.

Dennison et al. (2006) modeled fire temperature and fractional area in Airborne Visible Infrared Imaging Spectrometer (AVIRIS) data collected over a wildfire. A spectral library of emitted radiance endmembers was created for temperatures from 500 K to 1500 K using the MODTRAN radiative transfer model (Berk et al., 1989). A second spectral library of reflected solar radiance endmembers was collected from the AVIRIS image. Each AVIRIS pixel spectrum was modeled using the combination of an emitted radiance endmember, a reflected solar radiance endmember, and a shade endmember used to account for variations in reflectance and fractional cover of the other endmembers.

Eckmann et al. (2008) used a multiple endmember spectral mixing model to estimate fire temperature and fractional area in Moderate Resolution Imaging Spectroradiometer (MODIS) data. Using a similar approach to Dennison et al. (2006), they modeled emitted radiance endmembers using MODTRAN and selected background radiance endmembers from a MODIS image. Since MODIS data cover the MIR and TIR spectral regions, Eckmann et al. (2008) used a shade endmember that incorporated scattered atmospheric radiance in the absence of an emitting background surface. The shade endmember was modeled in MODTRAN using an assumed background temperature of 10 K. Eckmann et al. (2010) applied this methodology to modeling seasonal changes in fire temperature and fraction area in MODIS data. Eckmann et al. (2009) applied a multiple endmember model to estimating fire temperature and fractional area in Advanced Spaceborne Thermal Emission and Reflection Radiometer (ASTER) data, and compared the results to the results from a simpler approach based on the Dozier (1981) equation. Temperature and fractional area estimated by the two models were similar, although the multiple endmember approach did produce higher temperature estimates in a few areas of the fire they analyzed.

While past use of linear spectral mixture modeling to retrieve fire temperature has commonly assumed that fire emitted radiance is single temperature blackbody emission, in reality, a fire burning within a sensor's instantaneous field of view will have many temperatures from multiple combusting fuel elements. The mixture of emitted radiance from multiple combusting fuel elements may or may not produce a spectral shape similar to that of a single temperature blackbody, depending on the area and proportion of temperatures within a pixel and the spectral region examined. Also, the emissivity of fire is dependent on pathlength through a flame, and the assumption of blackbody emissivity may only be valid for long pathlengths in excess of 6 m (Giglio & Kendall, 2001; Langaas, 1995). Comparison of temperature and fractional area modeled from different spectral regions can reveal whether the single temperature blackbody assumption produces consistent results across all wavelength regions.

3. Image data

The Indians Fire burned an approximately 300 km^2 area of the Santa Lucia Mountains in coastal central California, USA, in June, 2008. The fire was ignited by an escaped campfire on June 8, 2008, and rapidly spread under high wind conditions. At approximately 20:50 UTC on June 11, 2008, a NASA ER-2 high altitude aerial platform flew over the area during a period of high fire activity. Two instruments, AVIRIS and MASTER (MODIS/ASTER Airborne Simulator), simultaneously acquired data over the fire (Fig. 2).

AVIRIS collects 224 contiguous bands with 10 nm bandwidths covering an approximate spectral range of 360–2500 nm. An AVIRIS image containing the fire was delivered as a radiometrically calibrated product, with geometric correction and geographic referencing provided by an onboard global positioning system and inertial data (Boardman, 1999). The instantaneous field of view of AVIRIS is 1 mrad, which produced an image spatial resolution of 16.1 m.

MASTER spans a much wider spectral range than AVIRIS, having 50 bands with central wavelengths ranging from 0.46 to 12.9 µm. MASTER's average full width-half maximum bandwidth is approximately 0.05 µm in 25 bands covering the visible, NIR and SWIR spectral regions. Bandwidth averages are 0.15 µm in 15 MIR bands and 0.46 µm in 10 TIR bands. MASTER band characteristics are described in more detail in Hook et al. (2001). MASTER has an instantaneous field of view of 2.5 mrad, producing a spatial resolution two and a half times that of AVIRIS when the two sensors are flown at the same altitude. The MASTER image was delivered as a radiometrically calibrated product. MASTER MIR and TIR radiometric calibrations are based on two onboard blackbody references typically operated at 20 °C and 40 °C (Jeffrey Myers, personal communication). The MASTER image was not geometrically corrected and geographically referenced, so 362 tie points were used to register the MASTER image to the AVIRIS image. The MASTER image was then warped using triangulation, and resampled to a 40.25 m spatial resolution.

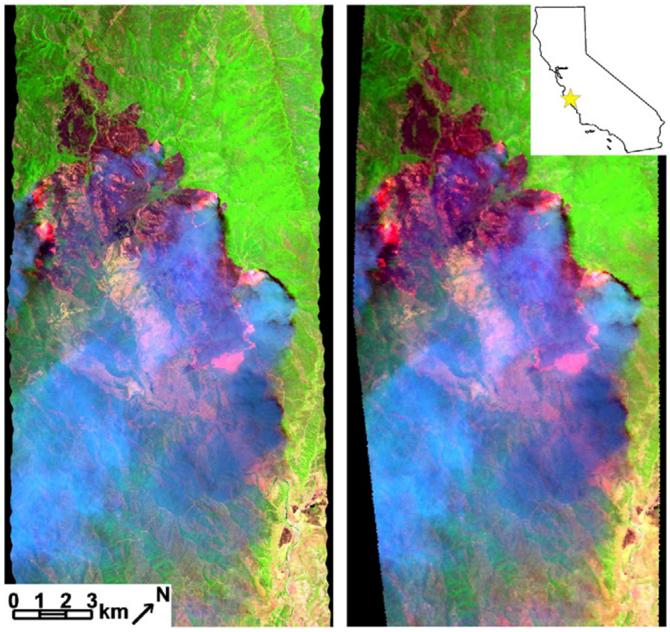

Fig. 2. AVIRIS (left) and MASTER (right) false color composites covering the Indians Fire. The AVIRIS composite uses bands centered at 1.672 µm (red), 0.957 µm (green), and 0.655 µm (blue). The MASTER composite uses bands centered at 1.668 µm (red), 0.952 µm (green), and 0.658 µm (blue). The yellow star on the inset map indicates the approximate geographic location of the images within the state of California.

AVIRIS and MASTER bands and spectra were visually inspected to determine whether water vapor absorption or scattering by smoke degraded emitted or reflected surface radiance. Bands with wavelengths shorter than 1.2 µm were discarded due to scattering by smoke. For both sensors, bands in major water vapor absorption features were also discarded. A total of 95 AVIRIS bands were selected for use in modeling. Three different models were run using MASTER data to determine how the wavelength regions covered by input radiance data affect fire temperature and fractional area retrieval. One model run used all SWIR, MIR, and TIR bands (24 bands total). A second MASTER model run used only the SWIR and MIR bands (18 bands total), while a third MASTER model run used only the MIR and TIR bands (13 bands total). The spectral coverage of AVIRIS and MASTER bands used for fire temperature and fractional area modeling is graphically depicted in Fig. 3.

4. Modeling

AVIRIS and MASTER pixel spectra were modeled with two- or three-endmember linear spectral mixing models. A fire detection index (Dennison & Roberts, 2009, see Section 4.3) was used to flag pixels that potentially contained emitted radiance from fire. Flagged pixels were

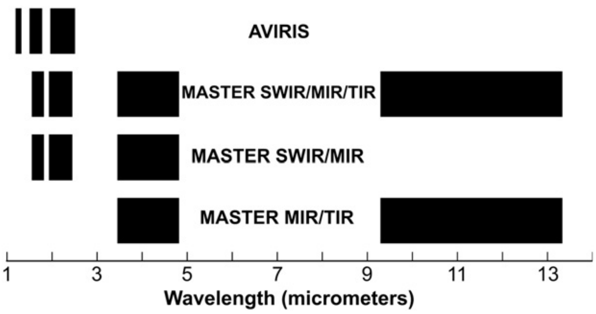

Fig. 3. Wavelength ranges (determined by band full width-half maximum values) covered by AVIRIS and MASTER bands used in temperature modeling.

modeled with a three-endmember model, with one endmember from a fire emitted radiance library, one endmember from a background library, and one "shade" endmember:

$$L_{\lambda sensor} = f_{Ef} L_{\lambda Ef} + f_b L_{\lambda b} + f_s L_{\lambda s} + \varepsilon_\lambda \tag{6}$$

where $L_{\lambda Ef}$ is the radiance of the fire emitted radiance endmember, $L_{\lambda b}$ is radiance of the background emitted and reflected radiance endmember, and $L_{\lambda s}$ is the radiance of a shade endmember that allows the fractions of the other two endmembers to vary and accounts for scattering by and emission from the atmosphere. f_{Ef}, f_b, and f_s are the fractional areas associated with each endmember. Unflagged pixels were modeled with a two-endmember model consisting of an endmember from a background library and the shade endmember:

$$L_{\lambda sensor} = f_b L_{\lambda b} + f_s L_{\lambda s} + \varepsilon_\lambda \tag{7}$$

The following sections describe fire emitted radiance endmember modeling, background radiance endmember selection, the fire detection index, and multiple endmember spectral mixture modeling.

4.1. Fire emitted radiance endmember modeling

MODTRAN 5.2 (Berk et al., 1989) was used to model fire emitted radiance and fire emitted path radiance for a range of temperatures from 300 K to 1500 K, at an interval of 10 K. To match the modeling assumptions used by previous efforts applying linear spectral mixture modeling to retrieving fire temperature, the emitting surface was assumed to be a blackbody. A mid-latitude summer atmospheric model with a visibility of 23 km was used. This visibility accurately approximated dark object reflected solar radiance outside of the smoke plume, but is likely much higher than actual visibility inside the smoke plume. However, reducing the modeled visibility down to 5 km resulted in no change in the emitted radiance endmembers at wavelengths longer than 1.2 μm. The atmospheric water vapor concentration was retrieved by running the AVIRIS image through ACORN (ImSpec LLC) reflectance retrieval software, which also produces a per-pixel atmospheric water vapor fit. An average water vapor concentration of 493 atm-cm in the area of the image containing the fire was used for emitted radiance modeling in MODTRAN. The modeled radiance spectra were convolved to AVIRIS and MASTER sensor response functions. The entire range (300–1500 K) of fire emitted radiance spectra was used to create the MASTER fire emitted radiance endmember library. Emitted radiance endmembers modeled for the 300–500 K temperature range can account for elevated temperatures following combustion and high background temperatures associated with sun-facing slopes and low solar albedo. It should be noted that pixels modeled by fire emitted radiance endmembers with temperatures less than 500 K may not actually contain fire. The AVIRIS fire emitted radiance endmember library was limited to temperatures between 500 and 1500 K, since temperatures cooler than 500 K do not reliably produce measureable radiance in the SWIR region (Dennison & Roberts, 2009).

4.2. Background endmember selection

The background radiance endmember accounted for reflected solar radiance, background emitted radiance, and reflected solar and background emitted contributions to path radiance. The multiple endmember spectral mixing model used a single background radiance endmember that was chosen from one of three background endmember libraries: a "non-smoke" background endmember library, a "smoke" background endmember library, and a "fire" background endmember library. Scattering by smoke can result in misclassification of background land cover (Dennison et al., 2006), so modeling in smoke-covered areas used a separate set of potential endmembers.

A simple smoke mask was generated for each image from a maximum likelihood classification. Regions of interest were created in the AVIRIS and MASTER images for 6 land cover classes in both smoke and non-smoke covered areas: oak/riparian woodland, chaparral/shrubland, grass, soil/rock, and two classes of ash. Two ash classes were necessary because of the spectral diversity in recently burned areas; some of these areas were spectrally flat in the SWIR, while other areas expressed absorption features that resembled ligno-cellulose absorption.

Smoke and non-smoke spectral libraries were extracted from the AVIRIS and MASTER regions of interest. An iterative endmember selection algorithm was used to model each library using MESMA. The endmember selection algorithm adds and subtracts endmembers with the goal of increasing accuracy, as measured through the kappa coefficient (Cohen, 1960), for all land cover classes within each library. Endmember selection was cut off at the point where increasing the number of endmembers resulted in minimal gains in kappa coefficient. A total of 10 non-smoke and 13 smoke endmembers were selected for modeling. A third background endmember library to be used when fire was detected within a pixel contained all of the non-green vegetation endmembers from the smoke endmember library. This fire background endmember library contained 8 endmembers.

4.3. Fire detection index

Dennison and Roberts (2009) demonstrated a Hyperspectral Fire Detection Index (HFDI) based on SWIR radiance at 2.06 and 2.43 μm. HFDI is calculated as:

$$\mathrm{HFDI} = \frac{\left(L_{2.43\mu m} - L_{2.06\mu m}\right)}{\left(L_{2.43\mu m} + L_{2.06\mu m}\right)} \tag{8}$$

As emitted radiance increases, radiance at 2.43 μm increases faster than radiance at 2.06 μm due to the shape of the Planck curve (Fig. 1). The addition of a small fractional area of fire to a pixel results in a large increase in HFDI. The main function of using a fire detection index in this case is to run the more efficient two endmember model that lacks a fire emitted radiance endmember for pixels that do not contain fire. Since fire may only occur in a small percentage of pixels, this can result in significant time savings in modeling an image (Dennison & Roberts, 2009). MASTER bands centered at 2.08 and 2.39 μm were used to calculate a similar fire detection index for the MASTER image. Index thresholds of 0.00 for the AVIRIS image and −0.196 for the MASTER image were empirically determined to separate burning pixels from non-burning pixels. Thresholds were set by adjusting the value of the threshold upward until no pixels outside of the apparent fire area were detected as burning.

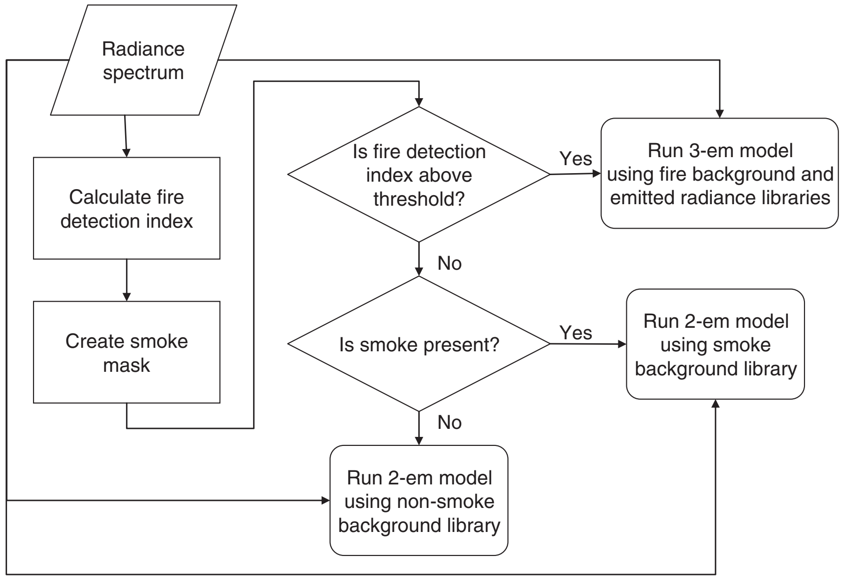

Fig. 4. A flowchart describing how the multiple endmember mixing model determines the number of endmembers (em) and the endmember libraries to use.

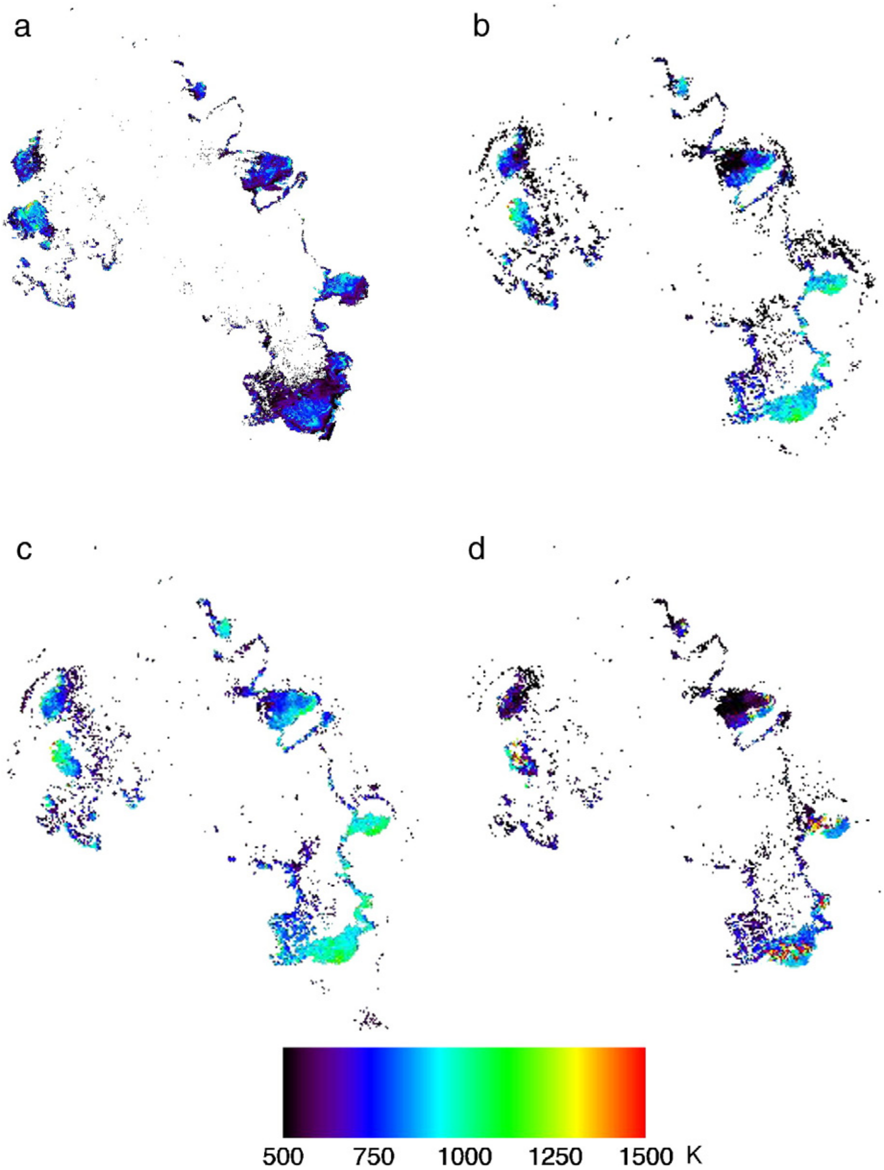

Fig. 5. Modeled temperature in Kelvin for AVIRIS (a), MASTER SWIR/MIR/TIR (b), MASTER SWIR/MIR (c), and MASTER MIR/TIR (d). Temperatures modeled below 500 K in the MASTER model runs are not shown for clarity.

4.4. Multiple endmember spectral mixture modeling

The smoke mask and fire detection index were used to determine which endmember libraries should be used to model each pixel (Fig. 4). Pixel spectra with fire detection index values above the detection threshold were modeled with a three endmember model using endmembers from the fire emitted radiance library and the fire background library, along with a shade endmember. Pixel spectra with fire detection index values below the threshold were modeled using two endmember models. For pixels flagged as having smoke present, the pixel spectrum was modeled with endmembers from the smoke background library and the shade endmember. If smoke was not present within a pixel, then the pixel spectrum was modeled with endmembers from the non-smoke background library.

Once the appropriate spectral libraries were determined for each pixel spectrum, the spectrum was fit by all possible combinations of endmembers from those libraries using singular value decomposition. A saturation spectrum for each sensor was used to screen out saturated bands, and pixel spectra were required to have two or more non-saturated bands for modeling. Endmember fractions were constrained to between 0 and 1; fractions exceeding either constraint were reset to the minimum or maximum fraction and residuals were calculated using that value (Dennison & Roberts, 2003). The endmember model producing the lowest RMSE was used to assign endmember identity, fractional area, and residuals to each pixel in the AVIRIS and MASTER images.

Temperatures and fire fractional areas were compared between four model runs: AVIRIS, MASTER SWIR/MIR/TIR, MASTER SWIR/MIR, and MASTER MIR/TIR (Fig. 3). Temperature and fractional area from the three MASTER model runs were directly compared pixel-to-pixel using linear regression and root mean square difference. Since the AVIRIS and MASTER data had different spatial resolutions, histograms of total area modeled at each fire temperature were used to compare all four model runs. For each pixel modeled at a specific fire temperature, the fire fractional area was multiplied by the pixel area. The total area at each temperature was then calculated by summing area across all pixels. Mean residuals at 500, 700, and 900 K were also determined for each model run. The Lee-Sallee shape index (Lee & Sallee, 1970) was used to compare the fire area, defined as the area with temperatures above 500 K, of each model run. Lee-Sallee is calculated as the ratio of the

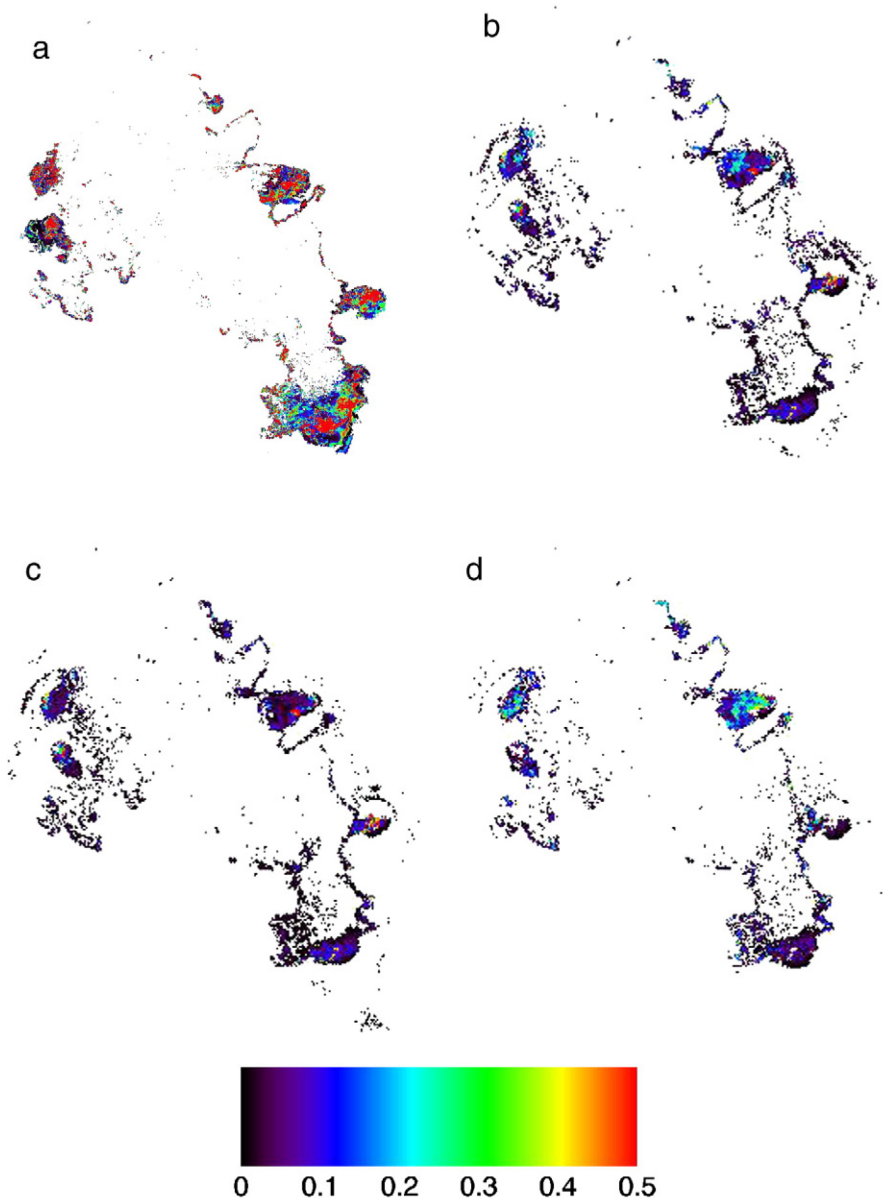

Fig. 6. Modeled fire fractional area for AVIRIS (a), MASTER SWIR/MIR/TIR (b), MASTER SWIR/MIR (c), and MASTER MIR/TIR (d).

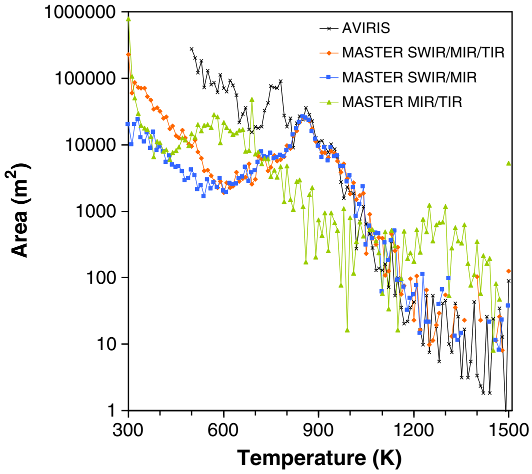

Fig. 7. Histograms showing total area modeled at each temperature. Note that the y-axis is scaled logarithmically. Temperatures for which no area was modeled are not shown, which produces "missing lines" between some individual points.

intersect of two areas to the union of two areas, and ranges between 0 (poor agreement) and 1 (total agreement). Since this metric is based on area, data having different spatial resolutions can be compared.

5. Results

All four model runs mapped high temperatures along the most active fire fronts within the Indians Fire (Fig. 5). The largest fire area was mapped by the AVIRIS model run, with much of the additional fire area (i.e. the area not mapped in the MASTER model runs) possessing temperatures at or slightly above 500 K. Both MASTER runs using SWIR bands mapped similar areas and temperatures (Fig. 5b and c). The MASTER MIR/TIR model run produced generally lower temperatures and the smallest fire area (Fig. 5d), although multiple pixels were modeled with a 1500 K temperature along the fire front in the lower right portion of Fig. 5d. These same areas were modeled at lower temperatures by the AVIRIS model run and by the MASTER model runs using SWIR data. In all four model runs, low temperatures were modeled ahead of the fire front in areas with higher emitted radiance produced by scattering rather than direct emission from the fire.

Due to the higher spatial resolution of AVIRIS, AVIRIS data were expected to produce higher fire fractional area values than MASTER data (Fig. 6). Fire fractional area exceeded 50% in much of the AVIRIS model run (Fig. 6a). In contrast, the model runs using MASTER data resulted in fire fractional areas below 10% over most of the fire, with small portions of the fire front exceeding 20% fractional area.

The four model runs demonstrated large differences in total area at each temperature for temperatures cooler than 800 K (Fig. 7). The AVIRIS model run produced a peak area at 500 K, the coolest emitted radiance endmember used in that model run. Additional peaks occurred at 780 K and 860 K. The two cooler peaks modeled from AVIRIS were not evident in any of the MASTER runs, but the third (and lowest) peak at 860 K corresponds with a similar peak at 850 K modeled from the MASTER SWIR/MIR/TIR and SWIR/MIR runs. The three model runs using SWIR data (AVIRIS, MASTER SWIR/MIR/TIR, and MASTER SWIR/MIR) show roughly similar distributions of total area at temperatures in excess of 820 K, although total area fluctuates widely at the hottest modeled temperatures. The MASTER MIR/TIR model run resulted in area peaks at 570 K and 690 K. Area also reached a lower peak in the 1250–1300 K range in the MIR/TIR model run, producing areas an order of magnitude higher in this temperature range than in any of the other model runs. Area modeled at 1500 K was much larger for the MIR/TIR model run than for the other model runs, with more than 5000 m^2 modeled at this temperature.

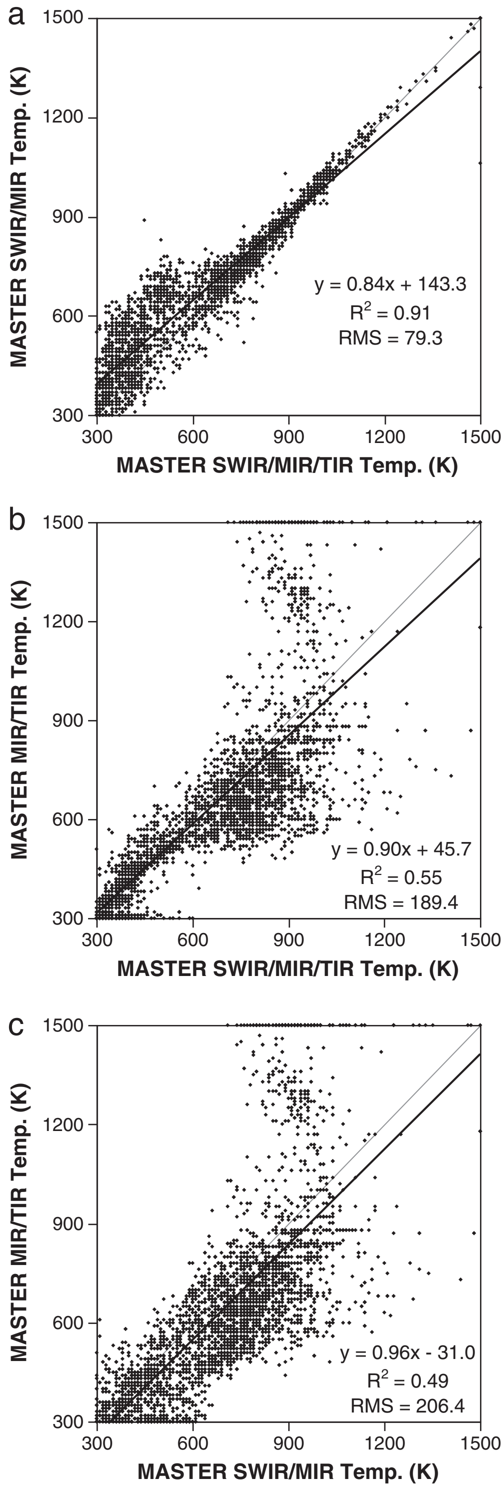

Fig. 8. Comparison of modeled temperatures for the MASTER model runs, including linear regression parameters and root mean square difference (RMS).

Temperature and fire fractional area were directly compared for pixels modeled by the three MASTER model runs (Figs. 8 and 9). The closest agreement in modeled temperature occurred for the SWIR/MIR/TIR and SWIR/MIR model runs (Fig. 8a). The SWIR/MIR model run produced slightly higher temperatures than the SWIR/MIR/TIR

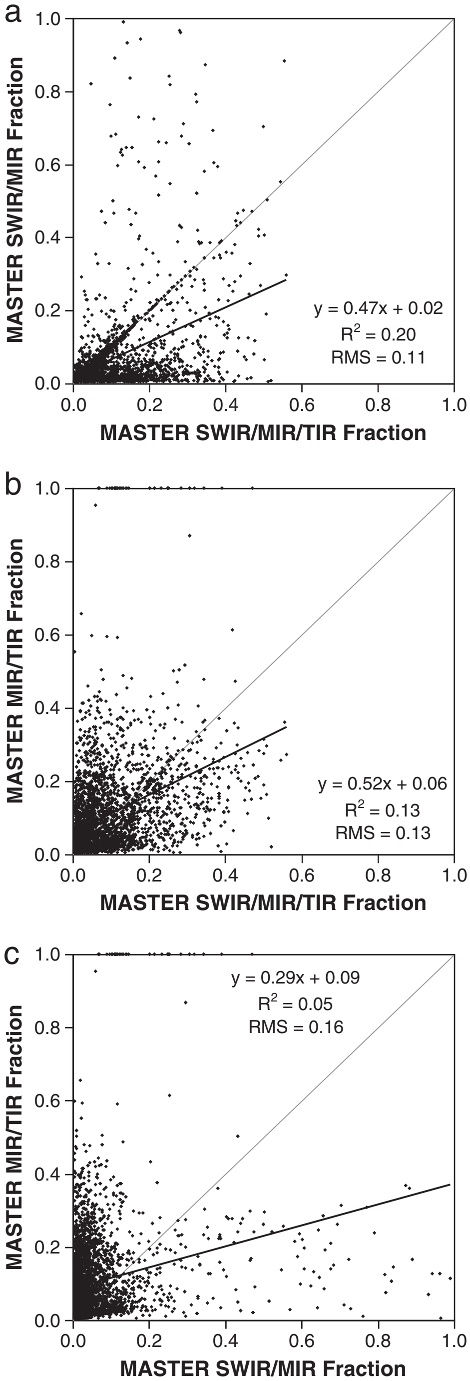

Fig. 9. Comparison of modeled fire fractional area for the MASTER model runs, including linear regression parameters and root mean square difference (RMS).

model run for temperatures below 800 K, but demonstrated close agreement for temperatures above 800 K. A linear regression between temperatures retrieved by the two model runs produced an R^2 of 0.91, and the root mean square difference between modeled temperatures was 79.3 K. Temperatures retrieved by the MIR/TIR model run were less strongly correlated with the other two model runs (Fig. 8b and c). Root mean square differences between modeled temperatures increased to near 200 K. Pixels modeled between 700 K and 1100 K in the two model runs using SWIR bands were modeled at both lower and higher temperatures in the MIR/TIR model run. The large number of 1500 K temperature retrievals in the MIR/TIR model run is also apparent in Fig. 8b and c.

When all modeled temperatures were included, there was poor agreement in fire fractional area between different model runs (Fig. 9). R^2 values for these fire fractional area comparisons did not exceed 0.20, even in the case of the SWIR/MIR/TIR and SWIR/MIR comparison which had strongly correlated temperatures. Root mean square differences in fractional area ranged from 0.11 to 0.16. However, when fractional area was compared solely for modeled temperatures in excess of 800 K, fractional area was very strongly correlated for the SWIR/MIR/TIR and SWIR/MIR model runs (Fig. 10b). Excluding temperatures below 800 K also strengthened the correlation between temperatures modeled from these two runs, reducing the root mean square difference to 12.4 K (Fig. 10a). Excluding temperatures below 800 K did not improve correlations including the MIR/TIR fractional areas, however.

The mean residual plots reveal wavelengths at which the model residuals were consistently positive or negative (Fig. 11). Large positive residuals (measured radiance larger than modeled radiance) occurred near the edges of water vapor absorption features. For comparison, water vapor transmittance spectra convolved to AVIRIS and MASTER bands are also shown in Fig. 11. Mean residuals increased as modeled temperature increased, a result of the higher radiance occurring at elevated temperatures. Mean residuals were largest in the MASTER model runs that used SWIR bands and smallest in the MASTER MIR/TIR model run.

The closest agreement in fire area, defined as the total area of all pixels modeled with temperatures in excess of 500 K, occurred

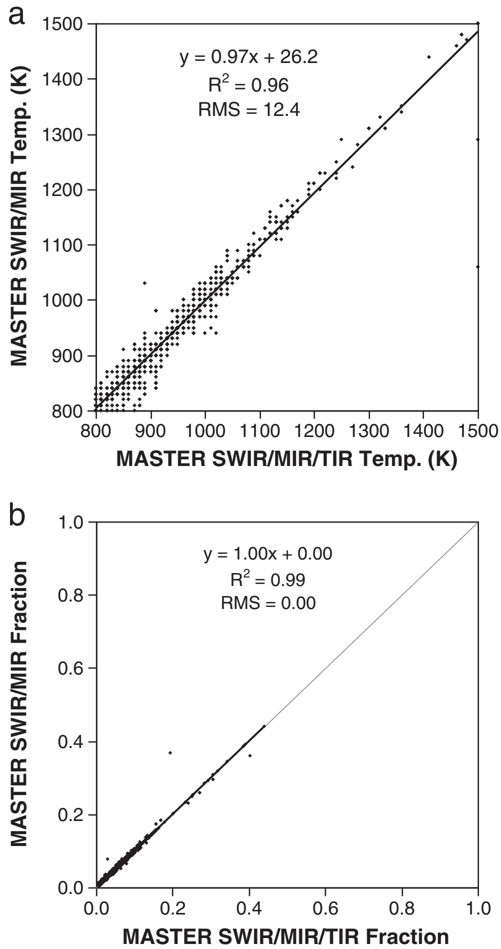

Fig. 10. Temperature (a) and fire fractional area (b) for the SWIR/MIR/TIR and SWIR/MIR model runs, excluding temperatures modeled below 800 K.

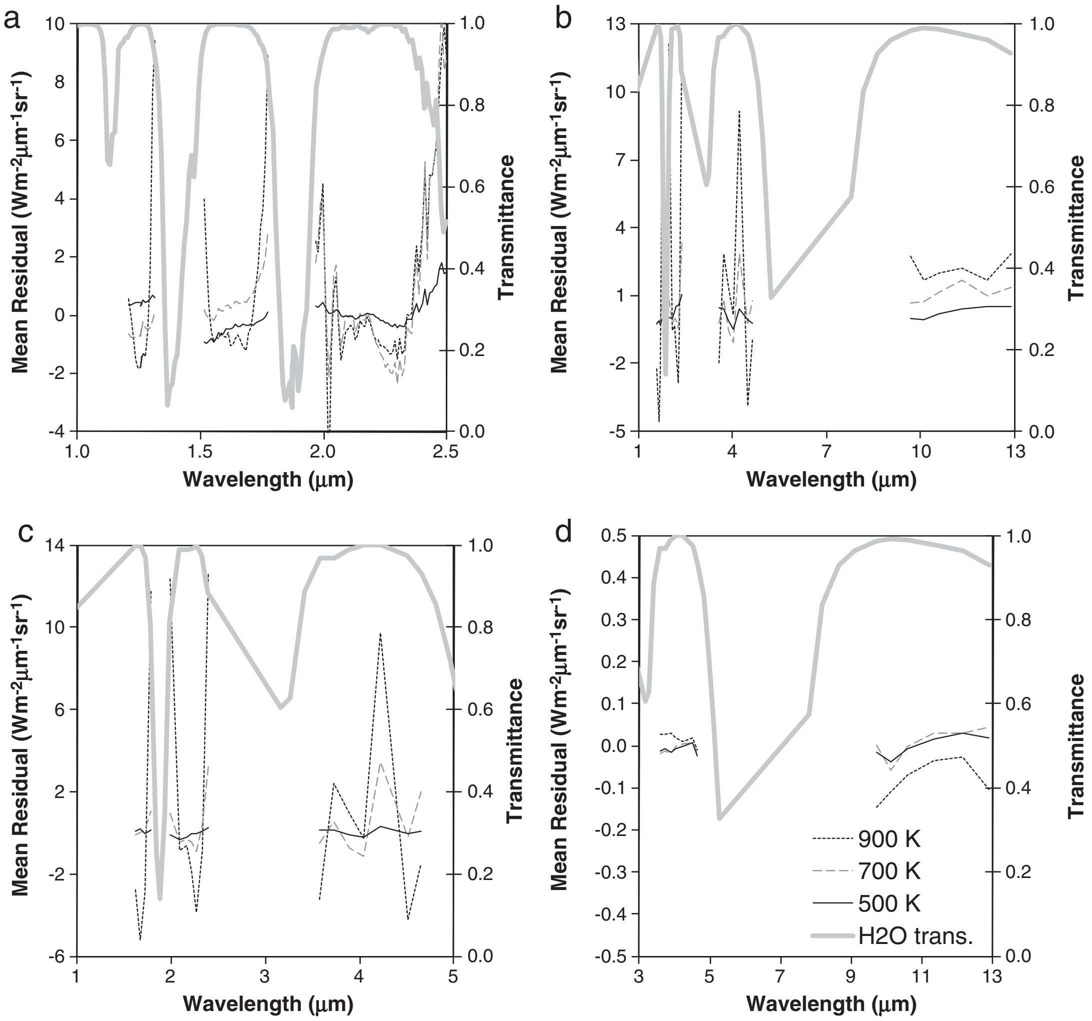

Fig. 11. Mean residual radiance (measured radiance–modeled radiance) for pixels at 500, 700, and 900 K from AVIRIS (a), MASTER SWIR/MIR/TIR (b), MASTER SWIR/MIR (c), and MASTER MIR/TIR (d). The modeled water vapor transmittance spectrum convolved to AVIRIS and MASTER bands is also shown with transmittance units on the right y-axis. The legend is in the lower right corner of plot (d).

between the MASTER SWIR/MIR/TIR and SWIR/MIR model runs (Table 1). Comparison of fire area mapped by AVIRIS model run with fire area mapped by the three MASTER model runs produced the lowest agreement, with Lee-Sallee values ranging from 0.416 to 0.451. The four model runs produced very different maps of background endmembers, as shown in Fig. 12. All four model runs mapped ash and soil within the fire scar, but the MASTER MIR/TIR model run mapped soil over a large area surrounding the fire. The MASTER model runs using SWIR bands erroneously mapped grass over a large area surrounding the fire. Qualitatively, the AVIRIS background endmember map most closely approximates land cover classes as they appear to be distributed in Fig. 2.

Table 1
Lee-Sallee values for areas mapped with temperatures higher than 500 K.

	MASTER SWIR/MIR/TIR	MASTER SWIR/MIR	MASTER MIR/TIR
AVIRIS	0.416	0.418	0.451
MASTER SWIR/MIR/TIR		0.671	0.621
MASTER SWIR/MIR			0.591

6. Discussion

Modeled fire temperatures and fractional areas were most consistent for model runs using AVIRIS and MASTER SWIR bands, and for modeled temperatures in excess of 800 K. Temperature and fractional area were less strongly correlated between model runs for lower temperatures and when the SWIR bands were excluded. Differences in modeled fire temperature and fractional area associated with wavelength and temperature are likely due to the dependence of emitted radiance on the latter two factors (Fig. 1). Differences in the spectral shape of emitted radiance are smaller at longer wavelengths, and can result in low temperature, high fractional area emission being spectrally similar to high temperature, low fractional area emission. The SWIR provides the greatest separability between low temperature and high temperature emission, resulting in more consistent modeled temperatures when SWIR bands are used. Within a single pixel, smoldering and flaming combustion across a wide range of temperatures will contribute to emitted radiance in the MIR and TIR. The resulting highly mixed emitted radiance may not be adequately modeled by a single temperature emitted radiance endmember. At shorter wavelengths, emitted radiance will be dominated by higher temperature flaming combustion. Emitted radiance in the SWIR should be less dependent on contributions

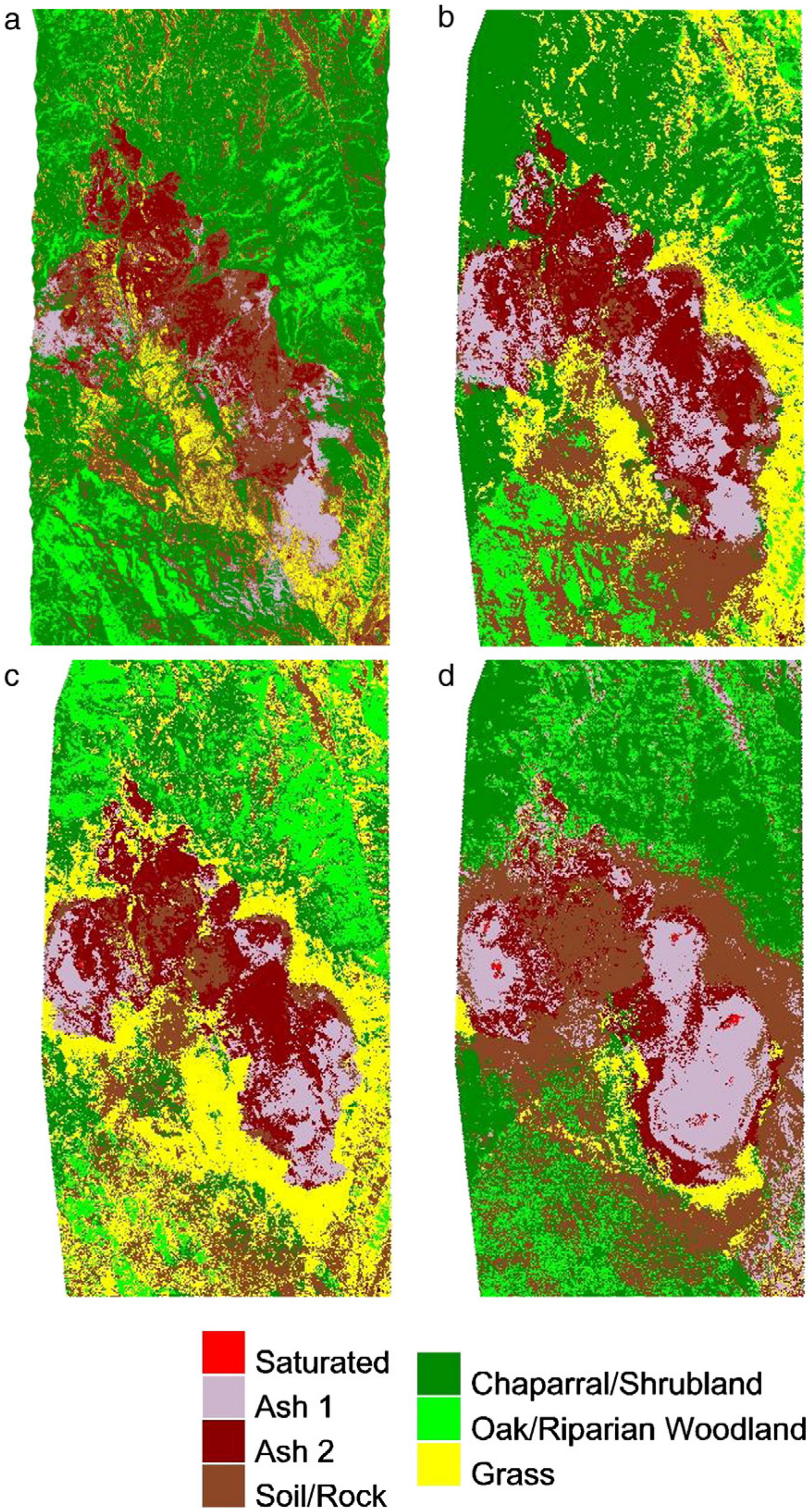

Fig. 12. Background endmembers mapped from AVIRIS (a), MASTER SWIR/MIR/TIR (b), MASTER SWIR/MIR (c), and MASTER MIR/TIR (d) data. "Ash 1" is ash lacking SWIR absorption features in the AVIRIS data, and "Ash 2" is ash exhibiting apparent lignocellulose absorption in the AVIRIS data.

from smoldering combustion, and emitted radiance from the highest combustion temperatures should dominate the emitted radiance signal.

Scattered emitted radiance produced overmapping of fire area in all four model runs. Radiance scattered ahead of the fire front resulted in low temperatures and fire fractional areas being mapped where the fire was likely not yet present. Screening out scattered emitted radiance may be difficult, however, because the scattered emitted radiance signal is very similar to the direct emitted radiance signal. Thresholding of lower temperatures and fire fractional areas can reduce the overmapping of fire where scattered emitted radiance is present, but this will also result in decreased mapping of smoldering combustion behind the fire front. Spectral shape, especially in the SWIR, could be used to map the background land cover, and pixels modeled as containing both fire and unburned vegetation could be flagged for potentially having scattered emitted radiance. Fire that has partially burned a canopy or is burning underneath a canopy could result in the same conditions, however.

Large, positive residuals adjacent to water vapor absorption features clearly indicate a shortcoming in modeling emitted radiance from fire and may have affected modeled fire temperature and fractional area. The combustion process produces large amounts of water vapor, and heated water vapor will have increased emitted radiance towards the edges of the atmospheric water vapor absorption features due to temperature broadening. Boulet et al. (2009) noted increased emitted radiance by heated water vapor in lab spectroscopy experiments, and also found a spike in emitted radiance near 4.5 μm caused by heated carbon monoxide and carbon dioxide that may explain the positive residual found near that wavelength in Fig. 11b and c. Accounting for variability in water vapor absorption and emission may be possible by varying the water vapor concentration modeled in emitted radiance endmembers. Additional emitted radiance endmembers will result in a greater number of potential endmember combinations in the spectral mixing model, which could greatly increase computational time. Per-pixel fitting of water vapor concentration before spectral unmixing would allow the selection of the best set of emitted radiance endmembers, and would partially mitigate the increased computational time.

7. Conclusions

Comparison of model runs using varying input wavelength regions demonstrated that fire temperature and fractional area were consistently modeled for fire temperatures in excess of 800 K when SWIR bands were included. The assumption that a single temperature blackbody emitted radiance endmember can be used to model fire temperature is potentially valid under these conditions, although the actual validity of this assumption cannot be determined using this dataset. Modeled fire temperature and fractional area were not in agreement for temperatures below 800 K and when SWIR bands were excluded. This limitation calls into question the abilities of spectral mixture modeling to accurately model the temperature of smoldering combustion. However, separation of flaming combustion from smoldering combustion, which cannot be done directly from radiance alone, may still be feasible.

Until further work can strongly link fire temperature and fractional area retrieved from remotely sensed data to fire temperature and fractional area measured *in situ*, caution is warranted when equating modeled temperatures to the actual temperature of a fire, especially at modeled temperatures below 800 K. The limitations of single temperature blackbody emitted radiance endmembers used in spectral mixture modeling of fires demonstrate that fire temperature modeling could greatly benefit from improved understanding of the radiative properties of fire at multi-meter scale spatial resolutions. A combination of field and lab measurement, modeling, and remote sensing would be very useful for assessing the spectral characteristics of fire emitted radiance and how these characteristics change with image spatial resolution.

Hyperspectral SWIR data provide important advantages for modeling fire temperature. Discrimination of water vapor absorption features provides the ability to estimate atmospheric water vapor concentration, which can then be used to improve fire emitted radiance modeling. Hyperspectral SWIR data may allow more accurate mapping of background land cover with simultaneous fire temperature and fractional area retrieval. Hyperspectral SWIR data also provide a more detailed measurement of the spectral shape of emitted radiance, which could allow fitting of multiple fire emitted radiance endmembers or creation of integrated measures of emitted radiance. Larger collections of hyperspectral SWIR data, including both daytime and nighttime fires, are needed to further test and improve fire temperature modeling. The VSWIR spectrometer to be carried by the proposed NASA HyspIRI mission could provide a global hyperspectral SWIR dataset containing observations of thousands of fires.

References

Andreae, M. O., & Merlet, P. (2001). Emission of trace gases and aerosols from biomass burning. *Global Biogeochemical Cycles*, *15*, 955−966.

Berk, A., Bernstein, L. S., & Robertson, D. C. (1989). *MODTRAN: A moderate resolution model for LOWTRAN7, AFGL-TR-89-0122.* MA: Hanscom Air Force Base.

Boardman, J. W. (1999). Precision geocoding of low altitude AVIRIS data: lessons learned in 1998. *Summaries of the eighth JPL Airborne Earth Science Workshop*, *99-17*. (pp. 63−68)Pasadena: Jet Propulsion Laboratory, JPL Publication.

Boulet, P., Parent, G., Collin, A., Acem, Z., Porterie, B., Clerc, J. P., et al. (2009). Spectral emission of flames from laboratory-scale vegetation fires. *International Journal of Wildland Fire*, *18*, 875−884.

Brooks, M. L. (2002). Peak fire temperatures and effects on annual plants in the Mojave Desert. *Ecological Applications*, *12*, 1088−1102.

Cohen, J. (1960). A coefficient of agreement for nominal scales. *Educational and Psychological Measurement*, *20*, 37−46.

DeBano, L. F. (2000). The role of fire and soil heating on water repellency in wildland environments: A review. *Journal of Hydrology*, *231–232*, 195−206.

Dennison, P. E., Charoensiri, K., Roberts, D. A., Peterson, S. H., & Green, R. O. (2006). Wildfire temperature and land cover modeling using hyperspectral data. *Remote Sensing of Environment*, *100*, 212−222.

Dennison, P. E., & Roberts, D. A. (2003). Endmember selection for multiple endmember spectral mixture analysis using endmember average RMSE. *Remote Sensing of Environment*, *87*, 123−135.

Dennison, P. E., & Roberts, D. A. (2009). Daytime fire detection using airborne hyperspectral data. *Remote Sensing of Environment*, *113*, 1646−1657.

Dozier, J. (1981). A method for satellite identification of surface temperature fields of subpixel resolution. *Remote Sensing of Environment*, *11*, 221−229.

Drewa, P. B., Platt, W. J., & Moser, E. B. (2002). Fire effects on resprouting of shrubs in headwaters of Southeastern longleaf pine savannas. *Ecology*, *83*, 755−767.

Eckmann, T. C., Roberts, D. A., & Still, C. J. (2008). Using multiple endmember spectral mixture analysis to retrieve subpixel fire properties from MODIS. *Remote Sensing of Environment*, *112*, 3773−3783.

Eckmann, T. C., Roberts, D. A., & Still, C. J. (2009). Estimating subpixel fire sizes and temperatures from ASTER using multiple endmember spectral mixture analysis. *International Journal of Remote Sensing*, *30*, 5851−5864.

Eckmann, T. C., Still, C. J., Roberts, D. A., & Michaelsen, J. C. (2010). Variations in subpixel fire properties with season and land cover in Southern Africa. *Earth Interactions*, *14-006.*

Giglio, L., & Justice, C. O. (2003). Effect of wavelength selection on characterization of fire size and temperature. *International Journal of Remote Sensing*, *24*, 3515−3520.

Giglio, L., & Kendall, J. D. (2001). Application of the Dozier retrieval to wildfire characterization — A sensitivity analysis. *Remote Sensing of Environment*, *77*, 34−49.

Hook, S. J., Myers, J. J., Thome, K. J., Fitzgerald, M., & Kahle, A. B. (2001). The MODIS/ASTER airborne simulator (MASTER): A new instrument for earth science studies. *Remote Sensing of Environment*, *76*, 93−102.

Langaas, S. (1995). A critical review of sub-resolution fire detection techniques and principles using thermal satellite data. PhD thesis, Department of Geography, University of Oslo, Norway.

Lee, D., & Sallee, G. (1970). A method of measuring shape. *Geographical Review*, *60*, 555−563.

Matson, M., & Holben, B. (1987). Satellite detection of tropical burning in Brazil. *International Journal of Remote Sensing*, *8*, 509−516.

Odion, D. C., & Davis, F. W. (2000). Fire, soil heating, and the formation of vegetation patterns in chaparral. *Ecological Monographs*, *70*, 149−169.

Oertel, D., Zhukov, B., Thamm, H. P., Roehrig, J., & Orthmann, B. (2004). Space-borne high resolution fire remote sensing in Benin, West Africa. *International Journal of Remote Sensing*, *25*, 2209−2216.

Palacios-Orueta, A., Chuvieco, E., Parra, A., & Carmona-Moreno, C. (2005). Biomass burning emissions: A review of models using remote-sensing data. *Environmental Monitoring and Assessment*, *104*, 189−209.

Riggan, P. J., Tissell, R. G., Lockwood, R. N., Brass, J. A., Pereira, J. A. R., Miranda, H. S., et al. (2004). Remote measurement of energy and carbon flux from wildfires in Brazil. *Ecological Applications*, *14*, 855−872.

Roberts, D. A., Gardner, M., Church, R., Ustin, S., Scheer, G., & Green, R. O. (1998). Mapping chaparral in the Santa Monica Mountains using multiple endmember spectral mixture models. *Remote Sensing of Environment*, *65*, 267−279.

Wooster, M. J., Zhukov, B., & Oertel, D. (2003). Fire radiative energy for quantitative study of biomass burning: Derivation from the BIRD experimental satellite and comparison to MODIS fire products. *Remote Sensing of Environment*, *86*, 83−107.

Zhukov, B., Briess, K., Lorenz, E., Oertel, D., & Skrbek, W. (2005). Detection and analysis of high-temperature events in the BIRD mission. *Acta Astronautica*, *56*, 65−71.